Mod Pathol 38 (2025) 100624

MODERN PATHOLOGY

USCAP UNITED STATES AND CANADIAN ACADEMY OF PATHOLOGY
Creating a Better Pathologist

Journal homepage: https://modernpathology.org/

Research Article

Spatial Cancer-Immune Phenotypes Predict Shorter Recurrence-Free Survival in the No Specific Molecular Profile Molecular Subtype of Endometrial Carcinoma

Dario de Biase[a,b], Jacopo Lenzi[c], Claudio Ceccarelli[d], Thais Maloberti[a], Marco Grillini[e], Camelia Alexandra Coadă[f], Claudio Zamagni[g], Pierandrea De Iaco[h], Anna Myriam Perrone[h], Donatella Santini[e], Martin Köbel[i], Cheng-Han Lee[j], Giovanni Tallini[a,d], Antonio De Leo[a,d,*]

[a] *Solid Tumor Molecular Pathology Laboratory, IRCCS Azienda Ospedaliero-Universitaria di Bologna, Bologna, Italy;* [b] *Department of Pharmacy and Biotechnology (FaBit), University of Bologna, Bologna, Italy;* [c] *Department of Biomedical and Neuromotor Sciences, University of Bologna, Bologna, Italy;* [d] *Department of Medical and Surgical Sciences (DIMEC), University of Bologna, Bologna, Italy;* [e] *Pathology Unit, IRCCS Azienda Ospedaliero-Universitaria di Bologna, Bologna, Italy;* [f] *Department of Morpho-functional Sciences, University of Medicine and Pharmacy "Iuliu Hatieganu", Cluj-Napoca, Romania;* [g] *IRCCS Azienda Ospedaliero-Universitaria di Bologna, Bologna, Italy;* [h] *Division of Gynecologic Oncology, IRCCS Azienda Ospedaliero-Universitaria di Bologna, Bologna, Italy;* [i] *Department of Pathology and Laboratory Medicine, University of Calgary, Calgary, AB, Canada;* [j] *Department of Pathology and Laboratory Medicine, University of Alberta, Edmonton, AB, Canada*

ARTICLE INFO

Article history:
Received 29 April 2024
Revised 30 August 2024
Accepted 13 September 2024
Available online 24 September 2024

Keywords:
endometrial carcinoma
immune response
molecular classification
prognosis
spatial-cancer immune phenotype
tumor microenvironment

ABSTRACT

Compartmentation of the immune response into 3 main spatial cancer-immune phenotypes (SCIs) — inflamed, excluded, and desert — has been proposed as the main predictor of response to immune checkpoint inhibitors in solid tumors. The objective of the study was to define and characterize the SCI in a consecutive series of 213 endometrial carcinomas (ECs) by correlating it with molecular subtypes, clinicopathologic features, and prognosis. Immunohistochemistry (IHC) and next-generation sequencing were used to assign surrogate molecular EC subtypes: *POLE* mutant (*POLE*), mismatch repair deficient (MMRd), *TP53* mutant (p53abn), and no specific molecular profile (NSMP). Immune cell markers (CD20, CD3, CD8, CD68, PD-L1) were assessed by IHC on whole sections and quantified by digital image analysis to define the 3 SCIs. ECs were stratified into 4 molecular subtypes: 17 (8.0%) *POLE*, 68 (31.9%) MMRd, 42 (19.7%) p53abn, and 86 (40.4%) NSMP. SCI determination showed 105 (49.3%) inflamed, 62 (29.1%) desert, and 46 (25.6%) excluded tumors. The inflamed phenotype was more prevalent in MMRd (64.7%) and *POLE* (76.5%) subtypes compared with NSMP (45.3%) and p53abn (21.4%). SCI revealed a strong correlation with disease-free survival in NSMP tumors: inflamed 96.2%, desert 83.2%, and excluded 40.5%. The SCI prognostic impact was also maintained in NSMP cases treated with adjuvant therapy resulting in a significant difference in recurrence between the inflamed and excluded phenotypes. To simplify SCI determination, a subset of immune cell markers was selected as appropriate to define the 3 SCI patterns: high intraepithelial CD8 for the inflamed phenotype; CD68, CD20, and PD-L1 to discriminate between desert and excluded tumors. The integration of SCI into molecular classification could be a promising opportunity to improve the prognostic risk stratification of patients and may guide the therapeutic

These authors contributed equally to this work and share first authorship: Dario de Biase, Jacopo Lenzi, and Claudio Ceccarelli.

These authors contributed equally to this work and share last authorship: Giovanni Tallini and Antonio De Leo.

* Corresponding author.
E-mail address: antonio.deleo@unibo.it (A. De Leo).

https://doi.org/10.1016/j.modpat.2024.100624

approach, particularly in the NSMP subtype. Thus, the different patterns of immune response are a new prognostic parameter in the NSMP subtype.

Introduction

Endometrial carcinoma (EC) is the most common gynecologic cancer with annual incidence rates in Western countries ranging between 15 and 25 per 100,000 women.[1,2] Approximately 15% to 20% of patients with EC have high-risk diseases that follow an aggressive clinical course. In recent years, there has been significant advancement in the molecular understanding of EC. The Cancer Genome Atlas (TCGA) endometrial collaborative project identified the following 4 distinct prognostic EC subtypes based on the observed molecular alterations: (1) the ultramutated subtype, characterized by *POLE* exonuclease domain mutation (*POLE*), with an excellent prognosis; (2) the hypermutated subtype, defined by mismatch repair deficiency (MMRd) pathway, with an intermediate prognosis; (3) the copy-number high subtype, with *TP53* mutation (p53abn) associated with a poor prognosis; and (4) the copy-number low subtype, also known as no specific molecular profile (NSMP) with intermediate prognosis.[3] Several groups have attempted to introduce the TCGA approach into clinical practice by using surrogate markers,[4,5] and the 2020 World Health Organization (WHO) classification of female genital tumor defines a diagnostic algorithm for the integrated histomolecular EC classification based on *POLE* mutation analysis and immunohistochemistry (IHC) for MMR and p53. In addition, the European Society of Gynecologic Oncology/European Society of Radiation Therapy and Oncology/European Society of Pathology (ESGO/ESTRO/ESP) committee recently proposed a new risk stratification system for EC patients that incorporates clinicopathologic and molecular features.[6,7] Clinical application of molecular classification represents a revolutionary milestone in the management of EC patients. Although the 4 TCGA subtypes provide an important framework for classification, the NSMP subtype (the most common EC) represents a molecularly heterogeneous group of tumors with variable alterations and divergent clinical outcomes.[8-10] There is thus an opportunity for further molecular and prognostic refinements, particularly from the perspective of tumor microenvironment (TME), which was not a major factor in the original TCGA analysis. TME can affect tumor growth, progression, and responses to therapies, especially immunotherapies, as infiltrating stromal and immune cells are the major components of TME and play a pivotal role in cancer biology. Many observations indicate that tumor-infiltrating lymphocytes (TILs) and their spatial localization have significant diagnostic and prognostic values in multiple types of solid tumors.[11] Emerging evidence now suggests that in addition to the presence and relative abundance of TILs, the cellular composition and activation state of TILs that correspond to different spatial distribution may contribute to clinical outcomes. In this regard, 3 main spatial cancer-immune phenotypes (SCIs) have been identified and recognized for their association with clinical outcome and/or response to immune checkpoint inhibitors in solid tumors: inflamed (also referred to as "hot"; characterized by the presence of intratumoral lymphocytes), excluded (also referred to as "altered"; lymphocytes are restricted to the invasive margin by adaptive resistance), and desert (also referred to as "cold"; characterized by an overall lack of lymphocytes and immunologic ignorance).[11,12] Although SCI analysis can provide further prognostic and predictive insights, SCI classification has not been applied in EC to date.

The objective of our study was to define and characterize the SCIs using IHC and digital pathology approach in a consecutive series of molecularly classified ECs, and to correlate them to clinicopathologic features and prognosis.

Material and Methods

Study Cohort and Clinicopathologic Data

The study was approved by the local research ethics committee—Comitato Etico-Area Vasta Emilia Centro (registration no. 27/2019/Sper/AOUBo and 10/2023/Sper/AOUBo). After providing informed consent, 213 consecutive patients underwent surgical hysterectomy with staging at the Division of Gynecologic Oncology of "IRCCS Azienda Ospedaliero-Universitaria di Bologna" (Bologna, Italy).[13] For each patient, a representative formalin-fixed paraffin-embedded tissue block was selected from files of the pathology unit of the same institution. All histology slides were reviewed by 2 expert gynecologic pathologists (D.S. and A.D.L.) to assess pathologic parameters. Age at diagnosis, body mass index, and clinicopathologic findings including follow-up data were collected in a comprehensive database. Median follow-up was 23 months extending to a maximum of 144 (12 years), and disease recurrence occurred in 36 patients (52×100 person-months). ECs were histologically classified according to the 2020 WHO classification of tumors[14,15]; a binary tumor grading was applied[16] and stage was assessed using standard 2009 International Federation of Gynecology and Obstetrics (FIGO 2009) criteria.[17] Lymphovascular space invasion (LVSI) was assessed by applying 3 tiers of semiquantitative scoring: no LVSI, focal (a single focus of LVSI recognized around the tumor), and substantial (diffuse or multifocal LVSI around the tumor).[18,19] The pattern of myometrial invasion was reported including the presence of microcystic, elongated, and fragmented (MELF) pattern[20] and/or the presence of single invasive cells or small groups of cells (tumor budding).[21] The presence of extensive tumor necrosis was reported; necrosis confined within glands or at the tumor surface was not scored.

Proliferation was assessed both as a mitotic index, expressed as the number of mitoses per 10 high-power fields, and by proliferative index (Ki-67) (see Immunohistochemistry).

Immunohistochemical Markers for Surrogate Molecular Classification and Proliferative Index

Immunohistochemical (IHC) evaluation of p53, MLH1, PMS2, MSH2, and MSH6 for surrogate classification according to the WHO algorithm was performed on a Benchmark Ultra platform using Ventana antibodies combined with the OptiView DAB detection systems (Ventana Diagnostic Systems) (Supplementary Table S1).

IHC staining of p53 was classified as normal (wild-type), or abnormal/mutant-like (p53abn) if one of the following aberrant patterns was present: overexpression, absent expression, or cytoplasmic staining.[22,23]

A tumor was defined as mismatch repair deficient (MMRd) if MLH1/PMS2 or MSH2/MSH6 were negative or if at least 1 of the 4 proteins (MLH1, PMS2, MSH2, and MSH6) was absent.[24,25]

Quantitative proliferative index (Ki-67) was assessed using image analysis with the IMAGE Pro Plus 5.1 software (Media Cybernetics Inc.) in at least 40 ×200 magnification fields, and expressed as the ratio (%) between the positive neoplastic cells and the total neoplastic cells.[26]

Immunohistochemical Marker Staining and Scoring

IHC for CD68, CD20, CD3, CD8, and PD-L1 was performed on the most representative whole-tissue section on a Ventana Benchmark Ultra platform. For PD-L1/CD68, CD20/CD3 double staining was performed using the OptiView DAB detection kit (brown color) for visualization of the first immunostaining and the UltraView RED alkaline phosphatase detection kit (red color) for the second. A single CD8 staining was performed using the DAB kit. Sections were counterstained using hematoxylin and bluing reagent following Ventana indications. All reagents and antibodies were from Ventana Medical Systems. Staining protocols are summarized in Supplementary Table S1.

To identify the 3 main SCIs (immune-desert, immune-inflamed, and immune-excluded),[11] the evaluation was restricted to the tumor epithelium–peritumoral stroma interface: the tumor invasive front (Fig. 1). Detection of the tissue histologic structures was performed by an operator-guided definition of the tumor and peritumoral stroma. Digital images were taken from the entire tumor invasive front using a ×200 field (ocular 10/23 – objective Acroplan ×20/0.45 w.d.= 0.63 mm) on a Zeiss Axiskop 40 microscope (Carl Zeiss AG Oberkochen). The entire tumor invasive front was partitioned into ×200 fields, the number of which varied according to its size (from 43 to 184 fields). Each immune cell marker (CD68, CD20, CD3, CD8, and PD-L1) was quantified using the image cytometry software IMAGE Pro Plus V5.0.1 (Media Cybernetics Inc.). Their percentage index of positive staining was calculated by pixels of immunostained area/pixels of area of interest. The total inflammatory component was obtained by adding percentages of CD68, CD20, and CD3. Intraepithelial tumor-infiltrating $CD8^+$ lymphocytes ($CD8^+$iTILs) index was obtained by detecting 5 hotspots in the entire tumor area at ×200 fields. The percentage index of $CD8^+$iTILs was expressed as the ratio of CD8-positive intraepithelial lymphocytes to the neoplastic population. All markers were binarized into low and high using the respective median as cutoff (Supplementary Material and Methods section).

Spatial Cancer-Immune Phenotype Determination

Categorization into the 3 SCIs – inflamed, desert, and excluded – was obtained using median cutoff values of total inflammatory component (CD68 + CD20 + CD3), PD-L1 expression, and $CD8^+$iTILs. A median split was used for 2 main reasons: first, to ensure an adequate size for each phenotype, thus preserving statistical power; second, to adopt a conservative and exploratory approach based on the sole distribution of immune cell markers, thus limiting the risk of overfitting.

The set of classes was then combined to obtain a categorization into the 3 basic SCIs as follows (Fig. 2). Inflamed tumors were defined by high $CD8^+$iTIL density. Excluded tumors were characterized by low $CD8^+$iTIL density, any PD-L1 value, and a high peritumoral inflammatory component. Desert tumors were characterized by low $CD8^+$iTIL density, low PD-L1, and low peritumoral inflammatory component.

DNA Extraction and Next-Generation Sequencing

DNA was extracted from formalin-fixed paraffin-embedded tissue starting from 2 to 4 10-μm thick sections, according to the

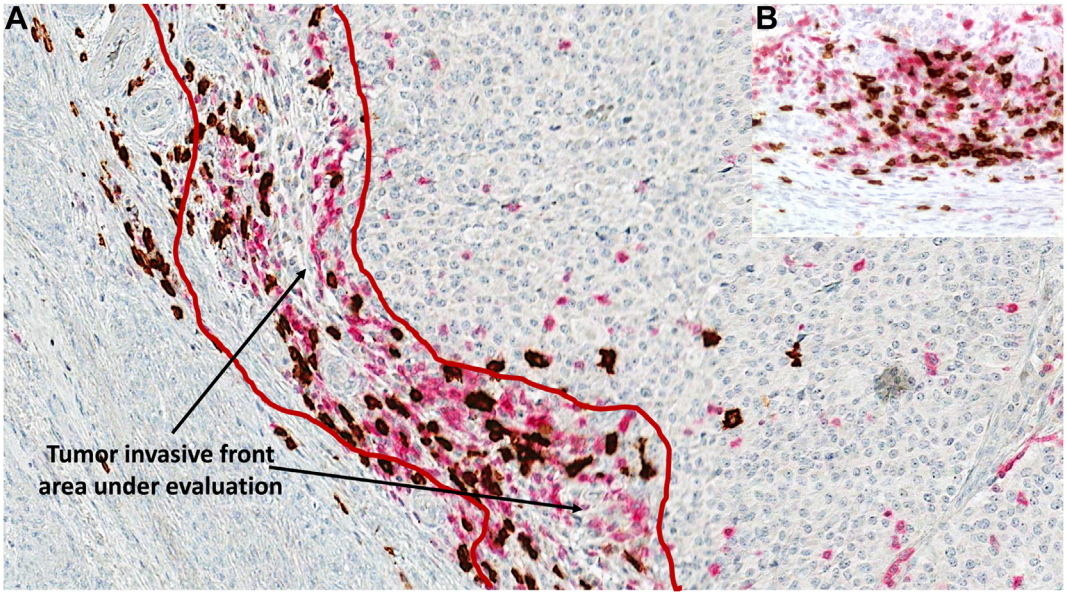

Figure 1.
Representative image of the tumor invasive front evaluated on whole slide: (A) area of evaluation (enclosed by red lines) stained for CD20 (brown) and CD3 (red); (B) ×200 magnification of the tumor invasive front used for digitally quantified immune cell markers.

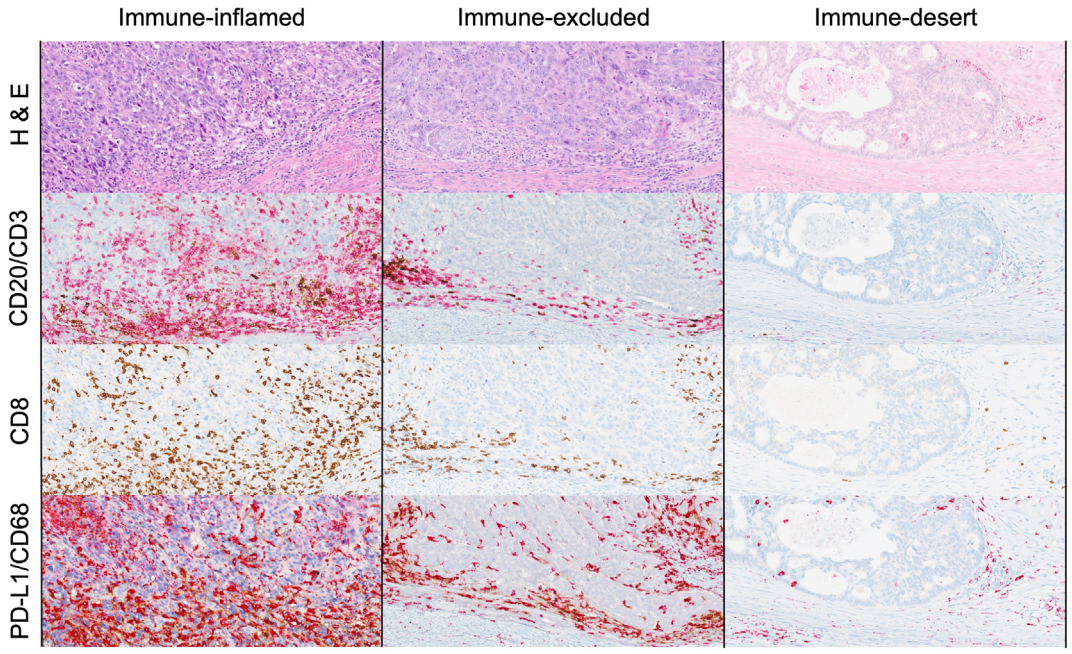

Figure 2.
Representative images of immune cell markers defining the 3 SCIs: inflamed, excluded, desert. Single immunostaining, CD8 brown color. Dual-marker immunostaining: CD20 brown color/CD3 red color; PD-L1 brown color/CD68 red color; (×200 magnification).

amount of tissue present in the paraffin block. The areas of interest were marked on the control hematoxylin and eosin-stained slide and manually dissected under microscopic guidance using a sterile blade. DNA was extracted using the Quick Extract Kit (LGC Biosearch Technologies) and quantified using the "Qubit" fluorometer (ThermoFisher Scientific). Samples were analyzed using a laboratory-developed multigene next-generation sequencing (NGS) panel of genomic regions and sequenced using the Gene Studio S5 Prime sequencer (ThermoFisher Scientific), according to the manufacturer's instruction as previously published.[27,28] Template preparation was performed using the Chef Machine instrument (ThermoFisher Scientific) and then sequenced using an Ion 530 chip. The panel included a total of 169 amplicons within the following gene regions (human reference sequence hg19/GRCh37, 12.74kb): *ARID1A* (complete coding sequence − CDS), *BRAF* (exon 15), *KIT* (exons 8, 9, 11, 13, 17), *CTNNB1* (exons 3, 7, 8), *HRAS* (exons 2-4), *KRAS* (exons 2-4), *NRAS* (exons 2-4), *PIK3CA* (exons 10, 21), *POLE* (exons 9-14), *TERT* (promoter region), and *TP53* (exons 2-9). Only nucleotide variations observed in at least 5% of the total number of reads analyzed were considered for mutational call. The sequences obtained were analyzed using the Ion Reporter Software (version 5.18, ThermoFisher Scientific) and the Integrative Genomics Viewer 2.12.2 (IGV) tool (Available online: http://software.broadinstitute.org/software/igv/).[29] The Varsome tool (https://varsome.com/.[30,31] was used to evaluate the classification of each mutation. *POLE* variants were evaluated according to Leon-Castillo et al[32] paper indications.

Molecular Classification of Endometrial Carcinoma

WHO Classification of Female Genital Tumors algorithm was applied.[15] Cases were classified as *POLE*, MMRd, NSMP, and p53abn. First, only pathogenic *POLE* mutations were used to assign the *POLE* subtype.[32] Then, consecutive IHC analysis for MMR proteins and p53 expression was evaluated to define MMR deficient (MMRd) and p53 abnormal (p53abn) tumors.[33] Tumors exhibiting normal p53 and MMR expression by IHC with no *POLE* mutations, were defined as NSMP tumors.

Statistical Analysis

Numerical variables were summarized as mean ± standard deviation (minimum to maximum); categorical variables were summarized as frequencies and percentages. Crude comparisons of baseline clinicopathologic characteristics across SCIs were performed using analysis of variance, Kruskal–Wallis test, χ^2 test, or Fisher exact test, as appropriate. The Kaplan–Meier estimator was used to display the time to relapse after surgery (ie, disease-free survival [DFS]) according to SCI and/or molecular subtype; the equality of survivor functions was assessed using the log-rank test or, in case the hazard functions were thought to vary in ways other than proportionally, the Wilcoxon–Breslow–Gehan test.[34,35] Loss to follow-up and study ending were treated as right-censored data; no premature deaths unrelated to the disease were observed during the study. Cox proportional-hazards regression analysis was used to investigate the association of baseline characteristics with DFS, forcing in the model established prognostic factors such as histology/grade (low-grade endometrioid EC vs high-grade endometrioid EC vs nonendometrioid/undifferentiated EC), FIGO 2009 stage (I/II vs III/IV), LVSI (absent/focal vs substantial), and molecular subtypes, and selecting other potential predictors listed in Table 1 with an automated stepwise procedure with significance levels of removal and addition equal to .05. The potential predictors included age, body mass index, depth of myometrial invasion, lymph node status, extensive tumor necrosis, MELF pattern of invasion, tumor budding, and therapy. Subsequently, SCI was added as an additional covariate, and its contribution to the model fit (ie, prediction accuracy for DFS) was quantified by means of the time-dependent Brier score obtained via inverse probability of censoring weighting.[36,37] The Brier score

Table 1
Clinicopathologic characteristics of the study sample, overall and by SCI evaluated at the tumor invasive front

Characteristics	All	Inflamed	Desert	Excluded	*P* value
	(n = 213)	(n = 105)	(n = 62)	(n = 46)	
Age, y	62.5 ± 10.5 (34-86)	62.7 ± 9.8 (36-81)	61.8 ± 11.1 (36-86)	63.0 ± 11.2 (34-80)	.82
Body mass index, kg/m^2	28.0 ± 7.2 (18.3-55.3)	28.5 ± 7.2 (18.34-55.3)	28.4 ± 7.7 (18.36-50.0)	26.3 ± 6.4 (19.33-51.1)	.19
Histotype/Grade					<.001[a]
EEC low grade	125 (58.7%)	73 (69.5%)	37 (59.7%)	15 (32.6%)	
EEC high grade	39 (18.3%)	18 (17.1%)	11 (17.7%)	10 (21.7%)	
Non-endometrioid/ Undifferentiated	49 (23.0%)	14 (13.3%)	14 (22.6%)	21 (45.7%)	
Molecular subtype					<.001[a]
POLE	17 (8.0%)	13 (12.4%)	2 (3.2%)	2 (4.3%)	
MMRd	68 (31.9%)	44 (41.9%)	7 (11.3%)	17 (37.0%)	
p53abn	42 (19.7%)	9 (8.6%)	17 (27.4%)	16 (34.8%)	
NSMP	86 (40.4%)	39 (37.1%)	36 (58.1%)	11 (23.9%)	
FIGO 2009 stage					.009[a]
IA	121 (56.8%)	64 (61.0%)	41 (66.1%)	16 (34.8%)	
IB/II	43 (20.2%)	20 (19.0%)	11 (17.7%)	12 (26.1%)	
III	40 (18.8%)	18 (17.1%)	6 (9.7%)	16 (34.8%)	
IV	9 (4.2%)	3 (2.9%)	4 (6.5%)	2 (4.3%)	
Depth of myometrial invasion, %					.008[a]
<50	150 (70.4%)	78 (74.3%)	48 (77.4%)	24 (52.2%)	
≥50	63 (29.6%)	27 (25.7%)	14 (22.6%)	22 (47.8%)	
Lymph node status					.27
Negative	177 (83.1%)	86 (81.9%)	56 (90.3%)	35 (76.1%)	
Positive	32 (15.0%)	16 (15.2%)	6 (9.7%)	10 (21.7%)	
Unknown	4 (1.9%)	3 (2.9%)	0 (0.0%)	1 (2.2%)	
Mitoses, 10 HPFs	53.5 ± 36.9 (1-230)	51.6 ± 37.9 (2-230)	43.1 ± 31.0 (1-120)	71.6 ± 36.2 (10-150)	<.001[a]
Ki-67, %	50.3 ± 20.0 (3.6-98.7)	49.2 ± 20.7 (3.6-98.7)	45.8 ±~ 18.9 (8.1-94.0)	59.0 ± 17.2 (26.6-87.6)	.002[a]
Extensive tumor necrosis					.002[a]
Absent	105 (49.3%)	59 (56.2%)	34 (54.8%)	12 (26.1%)	
Present	108 (50.7%)	46 (43.8%)	28 (45.2%)	34 (73.9%)	
MELF pattern of invasion					.001[a]
Absent	142 (66.7%)	59 (56.2%)	53 (85.5%)	30 (65.2%)	
Present	71 (33.3%)	46 (43.8%)	9 (14.5%)	16 (34.8%)	
Tumor budding					<.001*
Absent	122 (57.3%)	58 (55.2%)	48 (77.4%)	16 (34.8%)	
Present	91 (42.7%)	47 (44.8%)	14 (22.6%)	30 (65.2%)	
LVSI					.01
Absent/focal	136 (63.8%)	71 (67.6%)	44 (71.0%)	21 (45.7%)	
Substantial	77 (36.2%)	34 (32.4%)	18 (29.0%)	25 (54.3%)	
Therapy					.001[a]
Follow-up	81 (38.0%)	48 (45.7%)	28 (45.2%)	5 (10.9%)	
RT only[b]	47 (22.1%)	20 (19.0%)	14 (22.6%)	13 (28.3%)	
CHT only	16 (7.5%)	6 (5.7%)	3 (4.8%)	7 (15.2%)	
CHT + RT[b]	69 (32.4%)	31 (29.5%)	17 (27.4%)	21 (45.7%)	

Values are n (%) or mean ± standard deviation [minimum to maximum].
CHT, chemotherapy; EEC, endometrioid endometrial carcinoma; FIGO, 2009 International Federation of Gynecology and Obstetrics; HPF, high-power field; Ki-67, antigen Kiel 67; LVSI, lymphovascular space invasion; MELF, microcystic, elongated, fragmented; MMRd, mismatch repair deficient; NSMP, no specific molecular profile; p53abn, *TP53* mutant; *POLE*, *POLE* mutant; RT, radiotherapy; SCI, Spatial Cancer-Immune phenotype.
[a] *P* value ≤ .05.
[b] Either brachytherapy or external-beam radiation therapy, EBRT.

is an evaluation metric of disagreement computed as the average squared distance between the observed survival status and the predicted survival probability at specific time points and is always a number between 0 and 1, with 0 indicating a perfect fit (the lower the better). This implies that the inclusion of a strong prognostic factor into the model leads to a significant decrease in the Brier score, highlighting improved prediction accuracy. In our analysis, mean scores with 95% confidence intervals were computed at 12, 24, 36, and 48 months of follow-up. The proportional-hazards assumption was confirmed after checking for the nonzero slope of scaled Schoenfeld residuals on time. Model convergence was ensured by handling tied failures with exact marginal likelihood.

All post-hoc pairwise evaluations, including those involving Kaplan–Meier estimators, were performed using the multiple-test procedure proposed by Benjamini and Yekuteli to control the false discovery rate under arbitrary correlation between unadjusted *P* values.[38] This procedure transforms each *P* value into a *Q* value, sometimes known as "adjusted *P* value," which corresponds to the lowest uncorrected critical *P* value that would cause the input *P* value to be included in the discovery set if the specified multiple-test procedure was applied to the full vector

of *P* values. The significance threshold for *Q* values is the original .05.

Lastly, subgroup analyses were conducted according to therapy (follow-up vs radiotherapy only either brachytherapy or external-beam radiation therapy vs chemotherapy only [carboplatin alone or in combination with taxane] vs chemotherapy plus radiotherapy) and MMRd status (*MLH1* promoter-methylated vs Lynch syndrome/somatic mutation cases). All analyses were carried out using Stata software, version 17 (StataCorp. 2021. *Stata Statistical Software: Release 17* StataCorp LLC). The significance level was set at .05.

Results

Clinicopathologic Characteristics and Spatial Cancer-Immune Phenotypes

The application of the EC molecular algorithm allowed the classification of the 213 study patients into 4 surrogate molecular subtypes: 17 (8.0%) *POLE*, 68 (31.9%) MMRd, 42 (19.7%) p53abn, and 86 (40.4%) NSMP. Associations of molecular subtypes with clinicopathologic features are consistent with what has been reported in the literature (see Supplementary Table S2).

The distribution of SCIs was as follows: 105 (49.3%) inflamed, 62 (29.1%) desert, and 46 (21.6%) excluded tumors. The percentage of immune cell markers for each SCI is reported in Supplementary Table S3 and Supplementary Figure S1. Inflamed and excluded tumors showed a similar distribution of all immune cell markers evaluated at the tumor invasive front (CD68, CD20, CD3, and PD-L1). PD-L1 immunopositivity was mainly observed in the inflammatory cells with only 48 out of 213 (22.5%) cases also showing staining in tumor epithelium. Associations of SCIs with clinicopathologic characteristics are detailed in Table 1. The excluded phenotype was associated with aggressive histotype, advanced stage, deeper depth of invasion, higher mitotic count and Ki-67, extensive tumor necrosis, and substantial LVSI. Furthermore, SCIs were correlated with distinct patterns of invasion: (1) inflamed and excluded phenotypes were commonly characterized by the presence of MELF (43.8% and 34.8%, respectively), in contrast to desert cases in which this pattern was predominantly absent (14.5%); and (2) the presence of tumor budding showed a stepwise increase from desert (22.6%) to inflamed (44.8%), reaching the highest rate in the excluded phenotype (65.2%). Considering adjuvant therapy, immune-excluded tumors were most commonly treated with a combination of radiotherapy and chemotherapy.

Molecular Subtypes and Spatial Cancer-Immune Phenotypes

The frequency of the total inflammatory component and expression of individual immune cell markers by molecular subtypes of endometrial carcinoma is shown in Figure 3 and Supplementary Table S4. The *POLE* and MMRd subtypes both showed high percentages of immune cell markers compared with the p53abn and NSMP. The NSMP subtype showed consistently lower expression of immune cell markers than the others, except for $CD8^+$iTILs, which was significantly higher compared with p53abn tumors (Q value = .03). As shown in Table 1, the 3 SCIs were differently distributed across molecular subtypes. *POLE* and MMRd tumors were most commonly inflamed (76.5% and 64.7%, respectively), whereas p53abn cases mostly split between excluded and desert (38.1% and 40.5%, respectively), and NSMP

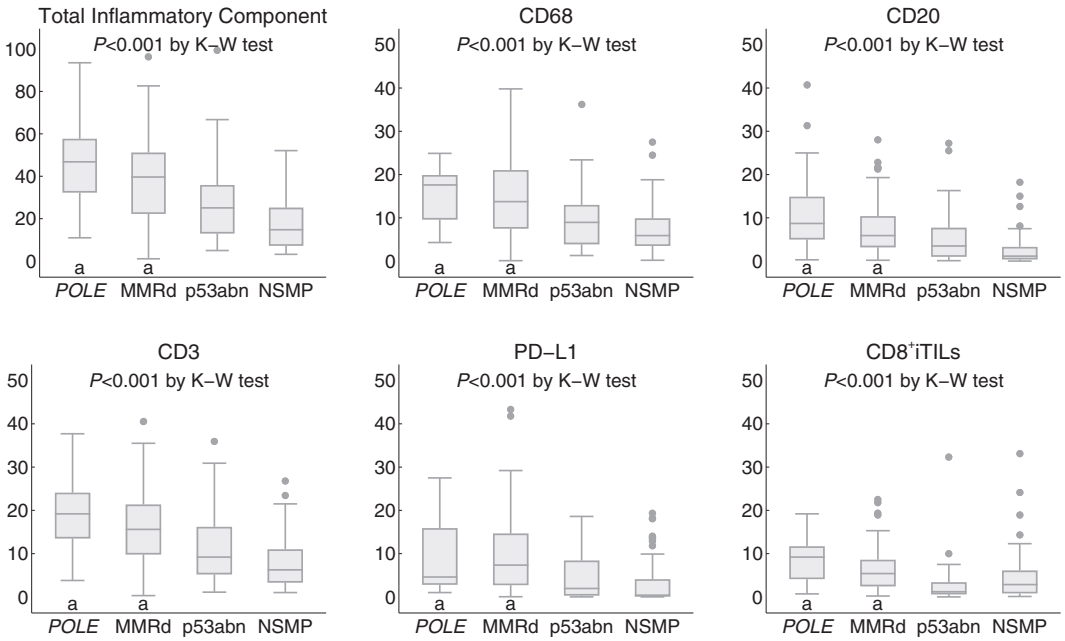

Figure 3.
Box-and-whisker plots showing the distribution of immune cell markers by molecular subtype. *Notes:* Pairs denoted with the same letter are not significantly different from each other at post-hoc evaluation. NSMP is significantly different from all other molecular subtypes, ie, *POLE* (total inflammatory component: Q value < .001; CD68: Q value < .001; CD20: Q value < .001; CD3: Q value < .001; PD-L1: Q value < .001; $CD8^+$iTILs: Q value = .01), MMRd (total inflammatory component: Q value < .001; CD68: Q value < .001; CD20: Q value < .001; CD3: Q value < .001; PD-L1: Q value < .001; $CD8^+$iTILs: Q value = .01), and p53abn (total inflammatory component: Q value = .005; CD68: Q value = .05; CD20: Q value = .008; CD3: Q value = .03; PD-L1: Q value = .05; $CD8^+$iTILs: Q value = .03). The whiskers of each plot stretch from the lower to the upper adjacent value, which corresponds to $Q_1 - 1.5 \times$ IQR and $Q_3 + 1.5 \times$ IQR, respectively. IQR, interquartile range; K–W, Kruskal–Wallis; MMRd, mismatch repair deficient; p53abn, *TP53* mutant; NSMP, no specific molecular profile; *POLE*, *POLE* mutant; Q_1, first quartile; Q_3, third quartile.

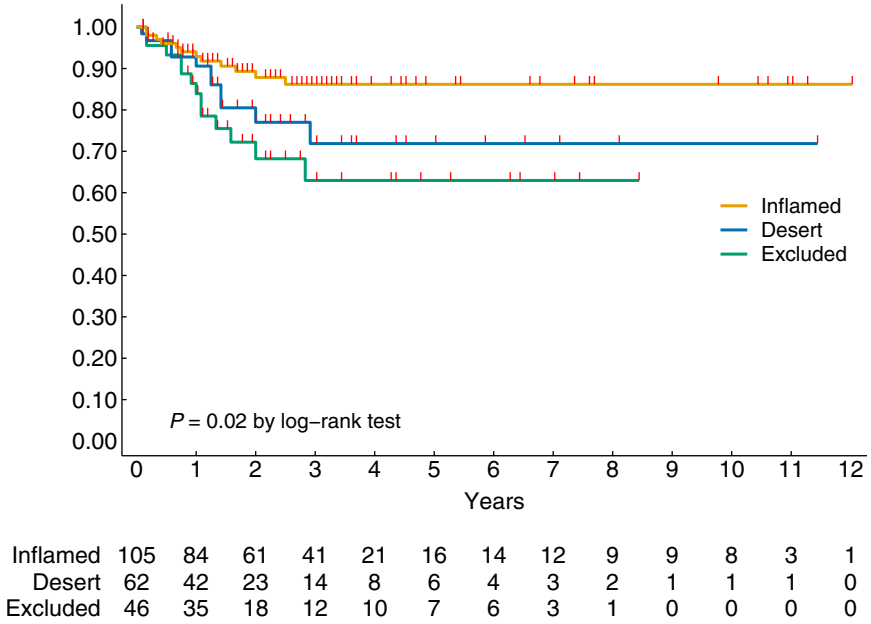

Figure 4.
Kaplan−Meier estimates of disease-free survival according to SCIs; censoring times are marked with red spikes. SCI, spatial cancer-immune phenotype.

cases between inflamed and desert (45.3% and 41.9%, respectively). We also subdivided the MMRd subtype into 2 subgroups: MLH1 promoter-methylated cases and Lynch syndrome/somatic mutation cases (see Supplementary Fig. S2). The total inflammatory component and CD20 were higher in Lynch syndrome/somatic mutation tumors, whereas the other immune cell markers showed no significant differences.

Prognostic Impact of Spatial Cancer-Immune Phenotypes

Molecular classification showed a statistically significant association with DFS, in line with the data reported in the literature (see Supplementary Fig. S3). The 3 SCIs showed significant differences in DFS, as shown in Figure 4. Inflamed tumors had a better prognosis, exhibiting a DFS of 86.2% (95% CI, 76.7-92.0); desert tumors had a DFS of 71.9% (95% CI, 52.9-84.3), whereas excluded tumors had the worst prognosis, with a DFS of 63.0% (95% CI, 43.2-77.5). Post-hoc pairwise analysis revealed a significant difference in DFS between inflamed and excluded phenotypes (Q value = .03), whereas no significant difference was found between inflamed and desert (Q value = .28) and between desert and excluded (Q value = .59).

In stratified analysis by molecular subtype (Fig. 5), SCIs were not significantly associated with DFS in *POLE*, MMRd, and p53abn subtypes.

In addition, splitting MMRd into MLH1 promoter-methylated cases and Lynch syndrome/somatic mutation cases, the prognosis was worse among MLH1 promoter-methylated tumors (but the log-rank test did not reach statistical significance due to the small sample size, see Supplementary Figure S4). Furthermore, no significant results emerged from the analysis of DFS according to SCIs in MMRd subgroups (see Supplementary Fig. S5).

In contrast, in NSMP tumors, SCIs revealed a strong correlation with DFS (P value < .001 by log-rank test). In particular, inflamed NSMP cases exhibited a DFS of 96.2% (95% CI, 75.7-99.5), desert NSMP cases 83.2% (95% CI, 60.7-93.5), and excluded NSMP cases 40.5% (95% CI, 10.0-70.1). Post-hoc pairwise analysis conducted on the NSMP subtype revealed a significant difference in DFS between inflamed and excluded phenotypes (Q value < .001) and between desert and excluded (Q value = .01), whereas no significant difference was found between inflamed and desert (Q value = 0.10).

Considering FIGO stages I and II EC cases (n = 164) (see Supplementary Fig. S6), not only excluded (Q value = .02) but also desert (Q value = .004) had a significantly worse prognosis as compared with the inflamed phenotype. When the analysis was further restricted to NSMP tumors with FIGO stages I and II (n = 77) (see Supplementary Fig. S7), the significant difference between inflamed and excluded phenotypes (Q value = .003) was confirmed also in this setting (early staged NSMP ECs).

In multivariable analysis aimed at estimating the prognostic value of the SCIs for the entire cohort in the context of other covariates − namely histotype/grade, FIGO 2009 stage, LVSI, and molecular subtype − histotype/grade and FIGO 2009 stage remained as independent parameters predictive of DFS, whereas SCIs were not statistically significant (see Table 2). When restricting the analysis to the NSMP molecular subtype (see Table 2), SCIs showed significant and independent association with disease recurrence, as well as substantial LVSI. In detail, desert and excluded phenotypes had a higher risk of recurrence than inflamed (desert: HR = 49.37, 95% CI, 2.92-834.86; excluded: HR = 46.68, 95% CI, 2.57-848.15), with no significant prognostic difference between them (P value = .96). Analysis by Brier score confirmed that SCI strongly improves the prediction model after 2 years of follow-up in the NSMP subtype, maintaining this prognostic impact over time (36 and 48 months) (see Fig. 6).

Considering the prognostic importance of SCI, we also aimed to simplify its classification approach to improve potential clinical implementation in routine practice. We have identified a selected subset of immune cell markers potentially adequate to classify tumors into the 3 SCI patterns: high $CD8^+$iTILs for immune-inflamed phenotype (by definition); CD68, CD20, and PD-L1 to

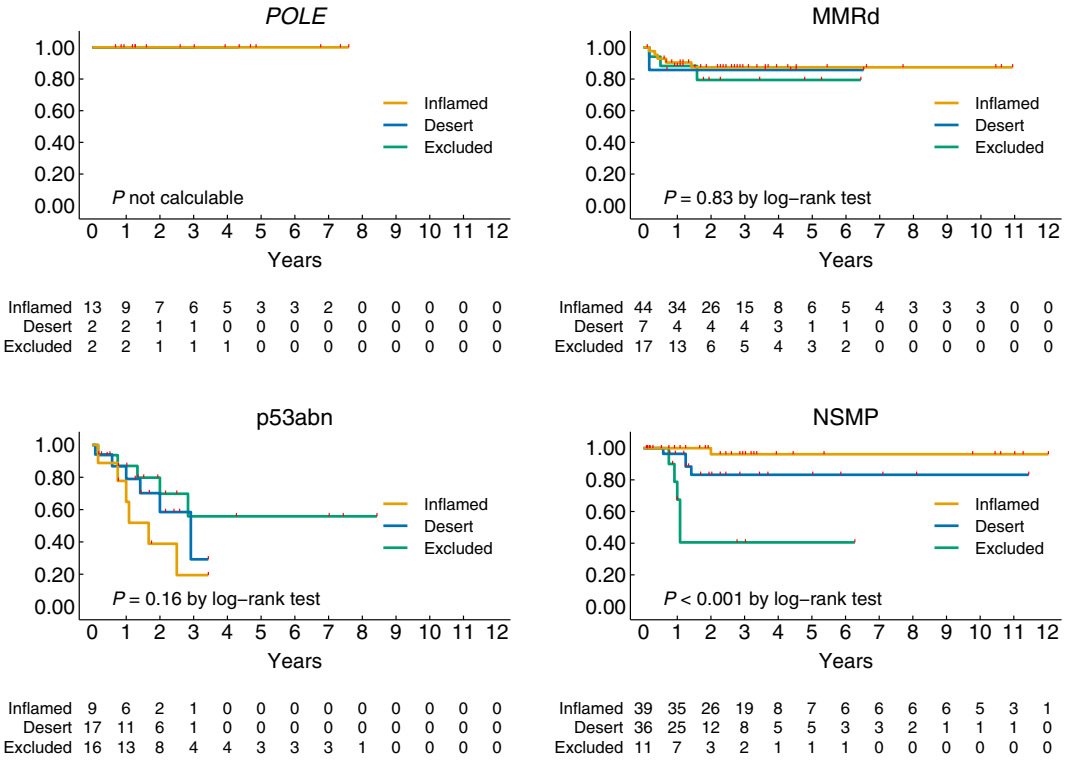

Figure 5.
Kaplan–Meier estimates of disease-free survival according to SCIs stratified by molecular subtype; censoring times are marked with red spikes. MMRd, mismatch repair deficient; NSMP, no specific molecular profile; *POLE*, *POLE* mutant; p53abn, *TP53* mutant; SCI, spatial cancer-immune phenotype;.

discriminate between immune-desert and immune-excluded tumors (see Supplementary Table S5). This simplified approach demonstrated high classification power as the model was able to accurately identify SCI (201/213; 94.4% precision) showing consistent prognostic impact both for the entire cohort (log-rank: $\chi^2 = 6.4$, $P = .041$) and for NSMP only (log-rank: $\chi^2 = 15.51$, $P < .001$).

Spatial Cancer-Immune Phenotypes and Response to Adjuvant Therapy

We conducted subgroup survival analyses focusing on SCIs and adjuvant therapies: radiotherapy only, chemotherapy only, and combined chemotherapy and radiotherapy. Considering 132 cases that underwent therapy, there is no statistical difference between different SCIs, although a trend with better prognosis of immune-inflamed tumors was evident (Supplementary Fig S8). In contrast, Kaplan–Meier estimates of DFS according to SCI stratified by treatment showed better prognosis of immune-inflamed tumors treated with radiotherapy only (Supplementary Fig. S9). Restricting the analysis to NSMP cases treated with adjuvant therapy (37 cases), the post-hoc pairwise analysis revealed a significant difference in recurrence between inflamed and excluded phenotypes (Q value $= .002$). Results were confirmed after adjustment for histotype/grade, FIGO stage, and LVSI via Cox regression (Fig. 7).

We also included therapy in the list of potential predictors for the Brier score analysis; however, the variable was omitted through stepwise regression, leaving the final results unchanged (data not shown).

Discussion

In recent years, the therapeutic advancements in cancer immunotherapy have highlighted the importance of a thorough understanding of the relationship between the human immune system and cancer and in investigating the role of immune cells in tumor progression and the tumor mechanisms of evading the immune response.[39,40] Comprehension of the molecular mechanisms that contribute to the suppression of the immune response against tumor-associated neoantigens is critical in clinical practice, as a plethora of immune checkpoint blockers/agonists or PD1/PD-L1 inhibitors have been introduced into clinical oncology, providing a new therapeutic approach in several cancer types. Nevertheless, only a subset of patients experiences durable responses, reflecting the underlying complexity of immuno-oncology.[41] The spatial distribution of immune cells in the TME can be segregated into 3 main SCIs: the desert phenotype, marked by scant immune cells, particularly T cells, as a result of a defect in T-cell priming or activation and resulting in immunologic ignorance; the inflamed phenotype, characterized by the presence of a significant number of subtypes of immune cells together with tumor-infiltrating lymphocytes ($CD8^+$TILs); the excluded/altered phenotype, also characterized by the presence of abundant immune cells, but in contrast to the inflamed phenotype, confined in the stroma surrounding the tumor, suggesting some form of adaptive resistance.[11,12,42] These histologically defined SCIs provide a useful framework to profile immune contexture in solid tumors and may give more nuanced insights into how cancer cells interact with immune cells spatially.[43]

In applying this SCI analysis to our EC cohort in relation to conventional clinicopathologic parameters, surrogate molecular

Table 2
Cox proportional-hazards regression analysis of disease-free survival in the overall sample and in the NSMP molecular subtype; mean Brier scores at 12, 24, 36, and 48 months are provided at the bottom of the table

Characteristics	Entire cohort (n = 213)						NSMP subtype (n = 86)					
	Without SCI			With SCI			Without SCI			With SCI		
	HR	*P* value	95% CI	HR	*P* value	95% CI	HR	*P* value	95% CI	HR	*P* value	95% CI
Histotype/grade												
EEC low grade	Ref.			Ref.			Ref.			Ref.		
EEC high grade	2.05	.22	0.65-6.47	1.99	.25	0.62-6.43	2.61	.34	0.37-18.59	6.85	.08	0.81-57.94
Nonendometrioid/undifferentiated	3.16	.03[a]	1.10-9.11	3.19	.04[a]	1.08-9.41	0.40	.45	0.04-4.27	0.68	.78	0.05-9.74
FIGO 2009 stage												
I/II	Ref.			Ref.			Ref.			Ref.		
III/IV	4.35	.001[a]	1.85-10.21	4.59	.001[a]	1.91-11.03	9.50	.02[a]	1.54-58.41	9.88	.08	0.78-125.27
LVSI												
Absent/focal	Ref.			Ref.			Ref.			Ref.		
Substantial	1.42	.44	0.58-3.50	1.41	.46	0.56-3.51	3.25	.21	0.52-20.21	8.68	.03[a]	1.28-58.74
Molecular subtype												
POLE	—	—	—	—	—	—	..	..	..	..	..	..
MMRd	0.54	.20	0.21-1.40	0.55	.22	0.21-1.44	..	..	..	..	..	..
p53abn	0.91	.84	0.34-2.39	0.88	.80	0.33-2.38	..	..	..	..	..	..
NSMP	Ref.			Ref.			Ref.			Ref.		
Extensive tumor necrosis												
Absent	Ref.			Ref.			Ref.			Ref.		
Present	.	.	.	.	.	.	13.69	.02[a]	1.46-128.11	7.33	.10	0.66-80.89
SCI												
Inflamed	Ref.			Ref.			Ref.			Ref.		
Desert	..	..	..	1.41	.43	0.60-3.30	..	..	..	49.37	.007[a]	2.92-834.86
Excluded	..	..	..	1.00	.99	0.42-2.40	..	..	..	46.68	.009[a]	2.57-848.15
Brier score												
12 months	0.075		0.047-0.102	0.075		0.047-0.102	0.034		0.000-0.070	0.037		0.000-0.077
24 months	0.108		0.071-0.144	0.110		0.073-0.147	0.059		0.014-0.103	0.037		0.000-0.075
36 months	0.111		0.074-0.148	0.115		0.074-0.155	0.063		0.015-0.111	0.037		0.000-0.075
48 months	0.110		0.072-0.149	0.119		0.069-0.170	0.070		0.014-0.125	0.040		0.001-0.079

Histotype, grade, FIGO stage, LVSI, and molecular subtype were selected for inclusion in Cox regression analysis as established predictors of disease-free survival. Em dash (—) means that no estimates were possible due to the absence of events in the *POLE* subtype. Single mid-dot (·) means that extensive necrosis was automatically discarded from the final model via stepwise regression, whereas double mid-dots (··) mean that SCI and/or molecular subtype were voluntarily discarded from the model.
CI, confidence interval; EEC, endometrioid endometrial carcinoma; FIGO, 2009 International Federation of Gynecology and Obstetrics; HR, hazard ratio; LVSI, lymphovascular space invasion; MMRd, mismatch repair deficient; NSMP; no specific molecular profile; p53abn, *TP53* mutant; *POLE*, *POLE* mutant; SCI, spatial cancer-immune phenotype.
[a] *P* value ≤ .05.

subtypes and their prognostic impact, we observed significant association between SCI patterns and several pathologic parameters. The most significant associations were seen with the excluded phenotype, which was strongly associated with adverse pathologic features such as aggressive histotypes, advanced stage, high-grade, deeper depth of invasion, high mitotic activity/

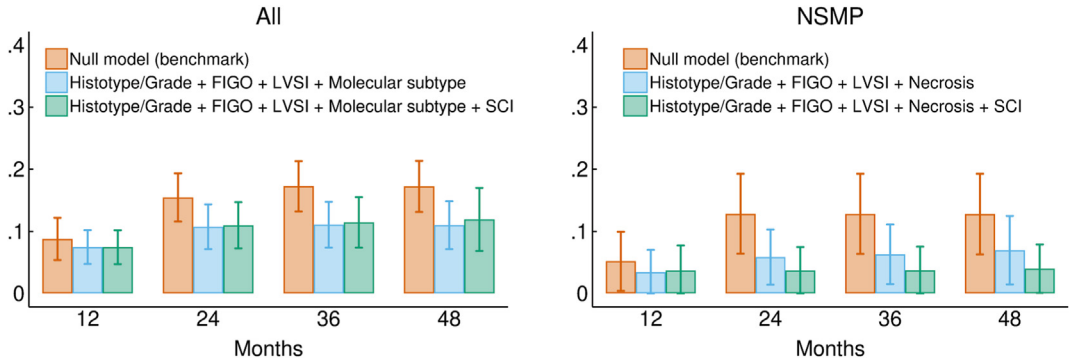

Figure 6.
Brier scores of semiparametric Cox regression models investigating disease-free survival and including different sets of predictors, starting from an empty (null) model that serves as a benchmark, overall and in the NSMP subtype. Mean scores with 95% confidence intervals are computed at 12, 24, 36, and 48 months of follow-up. *Notes:* Histotype, grade, FIGO 2009 stage, LVSI, and molecular subtype were selected for inclusion in Cox regression analysis as established predictors of disease-free survival, whereas extensive tumor necrosis was automatically selected via stepwise regression. No difference was observed in bar heights for the entire cohort after including SCI (first panel), whereas a consistent reduction in bar heights was observed after 2 years of follow-up for the NSMP subtype (second panel). FIGO, 2009 International Federation of Gynecology and Obstetrics; LVSI, lymphovascular space invasion; NSMP, no specific molecular profile; SCI, spatial cancer-immune phenotype.

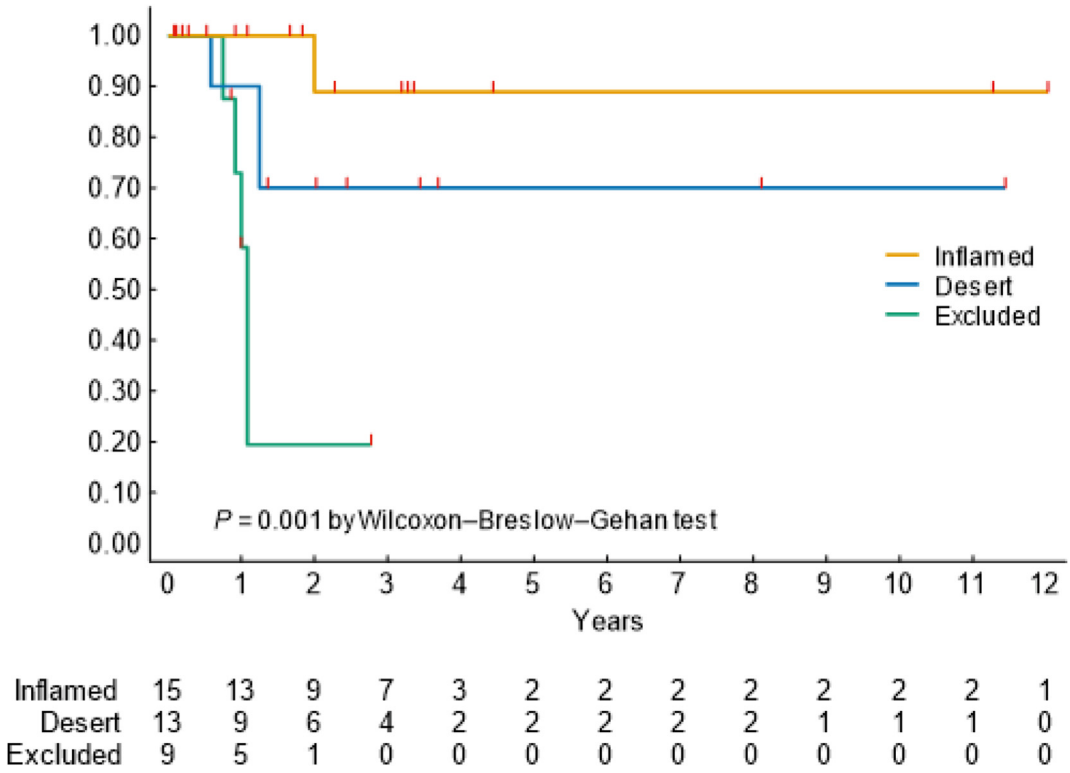

Figure 7.
Kaplan–Meier estimates of disease-free survival restricted to NSMP patients under therapy (n = 37) according to SCIs; censoring times are marked with red spikes. *Notes:* Post-hoc pairwise analysis revealed a significant difference in survival between inflamed and excluded phenotypes (*Q* value = .002). Results were confirmed after adjustment for histotype/grade, FIGO stage, and LVSI via Cox regression. FIGO, 2009 International Federation of Gynecology and Obstetrics; LVSI, lymphovascular space invasion; SCI, spatial cancer-immunophenotype.

proliferation index (Ki-67), extensive tumor necrosis, and substantial LVSI. Immune-inflamed and immune-excluded phenotypes showed significant associations with specific patterns of invasion, defined as MELF and tumor budding, whereas these invasion patterns were predominantly absent in immune-desert tumors. Thus, the inflammatory microenvironment at the tumor invasive front appears to be associated with the pattern of tumor invasion, as MELF and tumor budding are suggestive features of epithelial–mesenchymal transition.[44] The association of substantial LVSI only with immune-excluded cases suggests that this phenotype may be potentially associated with increased tumor dissemination. DFS analysis confirmed this difference in aggressiveness between immune-inflamed and immune-excluded tumors (DFS = 86.2% and 63.0%, respectively). However, at multivariable analysis including prognostic pathologic parameters (histotype/grade, stage, LVSI, and molecular subtype), these SCIs do not maintain statistical significance. Interestingly, the prognostic significance of SCIs changes when integrated into each molecular subtype. First, the distribution of the inflammatory component and immune cell markers showed no significant differences between *POLE* and MMRd molecular subtypes with the prevalence of immune-inflamed phenotype. In contrast, p53abn and NSMP cases exhibited distinct distributions of immune cell markers, both in relation to each other and when compared with the other molecular classes. The majority of p53abn tumors had immune-desert (40.5%) and immune-excluded phenotypes (38.1%), reflecting a significant absence of inflammatory components or, if present, a very low amount of $CD8^+$TILs. In NSMP cases, immune-inflamed (45.3%) and immune-desert (41.9%) were prevalent; when the inflammatory component is present, it is primarily linked to high $CD8^+$TILs. Prognostic evaluation of SCIs within each molecular subtype showed no prognostic value in *POLE*, MMRd, and p53abn cases, whereas a significant prognostic role of SCIs was particularly evident in the NSMP tumors. In this subtype, the immune-excluded phenotype is strongly associated with disease recurrence (DFS = 40.5%), immune-inflamed cases were almost free (DFS = 96.2%), and those with immune-desert exhibited an intermediate prognosis (DFS = 83.2%). Finally, on multivariate analysis we demonstrated that SCIs in NSMP subtype represented, together with LVSI, the only independent prognostic factors. Moreover, the prognostic value of the 3 SCIs persisted over time, as indicated by the Brier score analysis. Considering patients undergoing adjuvant treatment, the prognostic value of SCI did not reach statistical significance, although there was a trend showing that immune-inflamed cases tend to have a better prognosis. In addition, this trend was significant when the analysis is stratified by treatment: in patients treated with radiation therapy alone, the immune-inflamed phenotype was associated with a better response. Restricting the analysis to treated NSMP patients, the most remarkable finding was a different prognosis between immune-inflamed and immune-excluded cases, with the latter associated with poorer therapeutic response (regardless of type of therapy).

Several prior studies have evaluated the prognostic significance of the T-cell antitumor response in EC, which included approaches that classified the tumor immune microenvironment as T-cell-inflamed (hot tumors) or non–T-cell-inflamed (cold tumors).[45,46] A common system was to quantify the presence of $CD8^+$iTILs and identify its prognostic cutoff value. However, very few studies have evaluated this immune cell marker in the context

of TCGA molecular subtypes with conflicting results.[47,48] Limitations of previous works include the sole assessment of intraepithelial $CD8^+$ cell density, which does not allow a distinction between immune-desert and immune-excluded tumors, and the use of tissue microarrays that precludes a complete assessment of the spatial distribution of the inflammatory component. This distinction appears to be very relevant because, in our case series, only immune-excluded NSMP tumors have the worst prognosis, whereas immune-desert ones are less aggressive. A similar result on the aggressiveness of the excluded phenotype has recently been reported by López-Janeiro et al[49] based on a different methodological approach that did not include integration with EC molecular classification. Furthermore, beyond the prognostic importance of combining the SCIs with molecular subtypes, understanding of tumor-immune cell interaction in the specific TCGA EC molecular context may represent a more biologically accurate predictive parameter for the targeted immunotherapy. Recent evidence suggests a more likely response to immune checkpoint blockade therapies by tumors showing an immune-inflamed microenvironment, whereas both immune-desert and, fortiori, immune-excluded cases appear refractory to such therapy.[11,12,42,50-52] Currently, the factors responsible for immunosuppression in immune-excluded and immune-desert tumors are not fully identified, and immunotherapies capable of generating effective endogenous immunity in patients with these tumors are lacking. These latter phenotypes differ in their immune microenvironment: in immune-desert cases, the absence of immune response may be due to either immunologic ignorance, the induction of tolerance, or a lack of appropriate T-cell priming or activation (eg, HLA failure),[53] whereas in the immune-excluded phenotype, the blockade of effective anti−tumor-infiltrating T lymphocytes seems to be due to obstacles such as fibrosis and tumor cell-induced immunosuppression. That microenvironment is insufficient to trigger an effective immune response and is associated with increased biological aggressiveness, as demonstrated by the association between the excluded phenotype and the presence of remarkable proliferative activity (high mitotic count/Ki-67), peculiar pattern of invasion (MELF and tumor budding), substantial LVSI, which together confer an effective metastatic potential in NSMPs (40.5% of DFS).

Strengths of the present study include the enrollment of a homogeneous cohort with complete follow-up data and extensive annotation of molecular and pathological risk factors, and the use of whole-tissue sections, allowing a more thorough assessment of the density and spatial location of immune cells. Moreover, differently from other studies that commonly evaluate TILs, our approach highlights the importance of profiling the immune microenvironment by including an additional subset of immune cell markers such as CD68, PD-L1, and CD20 to define the SCIs.

Limitations of our study include the evaluation of a limited number of immune cell markers. On that note, it would be interesting to see if the analysis of additional immune cell types and markers of lymphocyte activation−exhaustion will improve prognostic stratification. Moreover, our findings require further validation in other cohorts. Furthermore, although numerous studies have demonstrated the high concordance between MMR IHC and microsatellite instability testing (>95%), in our cohort (classified by surrogate methodologies according to WHO) there might be a small but not insignificant number of cases (particularly in NSMPs) that might have microsatellite instability-H phenotype without IHC alteration of MMR.[25]

In summary, we found that SCIs derived by multiplexed IHC on whole section is strongly prognostic in the context of TCGA-based EC molecular classification. We demonstrated the diversity and heterogeneity of the immune response in different molecular subtypes and identified the prognostic importance of SCI patterns in the NSMP EC. In addition, a better understanding of SCI immune patterns could improve the therapeutic approach in EC in the era of immunotherapy, as recently demonstrated in other solid tumors.[50-52]

Acknowledgments

The authors would like to thank LOTO ONLUS Association, for supporting women's cancer research.

Author Contributions

A.D.L., C.C., and D.d.B. provided study concept and design; C.C., J.L., T.M., M.G., C.A.C., C.Z., A.M.P., P.D.I., and D.S. provided acquisition of data, analysis, and interpretation of data; A.D.L., D.d.B., C.C. drafted the manuscript; M.K., C.H.L, D.S., G.T. were involved in critical revision of the manuscript for important intellectual content; A.D.L. obtained funding; D.d.B., J.L., T.M., and C.A.C. provided technical or material support; and G.T. was involved in study supervision. All authors read and approved the final paper.

Data Availability

The data sets used and analyzed during the current study are available from the corresponding author upon reasonable request. Sequencing data sets presented in this study can be found in online repositories. The name of the repository and accession number can be found in NCBI Bioproject, PRJNA932605.

Funding

The research leading to these results has received funding from AIRC under MFAG 2021 − ID. 26319 project − P.I. De Leo Antonio.

Declaration of Competing Interest

The authors report no relevant conflicts of interest.

Ethics Approval and Consent to Participate

The study was approved by the local research ethics committee − Comitato Etico-Area Vasta Emilia Centro (CE-AVEC, registration n. 27/2019/Sper/AOUBo and 10/2023/Sper/AOUBo). Written informed consent was obtained from all the participants involved in this study, and all the clinical investigations were conducted in line with the principles of the Declaration of Helsinki.

Supplementary Material

The online version contains supplementary material available at https://doi.org/10.1016/j.modpat.2024.100624.

References

1. Allemani C, Matsuda T, Di Carlo V, et al. Global surveillance of trends in cancer survival 2000-14 (CONCORD-3): analysis of individual records for 37 513 025 patients diagnosed with one of 18 cancers from 322 population-based registries in 71 countries. *Lancet*. 2018;391:1023−1075. https://doi.org/10.1016/S0140-6736(17)33326-3
2. Ferlay J, Colombet M, Soerjomataram I, et al. Cancer incidence and mortality patterns in Europe: Estimates for 40 countries and 25 major cancers in 2018. *Eur J Cancer*. 2018;103:356−387. https://doi.org/10.1016/j.ejca.2018.07.005

3. Cancer Genome Atlas Research N, Kandoth C, Schultz N, et al. Integrated genomic characterization of endometrial carcinoma. *Nature*. 2013;497:67–73. https://doi.org/10.1038/nature12113
4. Stelloo E, Nout RA, Osse EM, et al. Improved risk assessment by integrating molecular and clinicopathological factors in early-stage endometrial cancer-combined analysis of the PORTEC cohorts. *Clin Cancer Res*. 2016;22:4215–4224. https://doi.org/10.1158/1078-0432.CCR-15-2878
5. Talhouk A, McConechy MK, Leung S, et al. A clinically applicable molecular-based classification for endometrial cancers. *Br J Cancer*. 2015;113:299–310. https://doi.org/10.1038/bjc.2015.190
6. Concin N, Matias-Guiu X, Vergote I, et al. ESGO/ESTRO/ESP guidelines for the management of patients with endometrial carcinoma. *Int J Gynecol Cancer*. 2021;31:12–39. https://doi.org/10.1136/ijgc-2020-002230
7. de Biase D, Maloberti T, Corradini AG, et al. Integrated clinicopathologic and molecular analysis of endometrial carcinoma: prognostic impact of the new ESGO-ESTRO-ESP endometrial cancer risk classification and proposal of histopathologic algorithm for its implementation in clinical practice. *Front Med (Lausanne)*. 2023;10, 1146499. https://doi.org/10.3389/fmed.2023.1146499
8. Jamieson A, Huvila J, Chiu D, et al. Grade and estrogen receptor expression identify a subset of no specific molecular profile endometrial carcinomas at a very low risk of disease-specific death. *Mod Pathol*. 2023;36, 100085. https://doi.org/10.1016/j.modpat.2022.100085
9. Vermij L, Jobsen JJ, Leon-Castillo A, et al. Prognostic refinement of NSMP high-risk endometrial cancers using oestrogen receptor immunohistochemistry. *Br J Cancer*. 2023;128:1360–1368. https://doi.org/10.1038/s41416-023-02141-0
10. Momeni-Boroujeni A, Nguyen B, Vanderbilt CM, et al. Genomic landscape of endometrial carcinomas of no specific molecular profile. *Mod Pathol*. 2022;35:1269–1278. https://doi.org/10.1038/s41379-022-01066-y
11. Chen DS, Mellman I. Elements of cancer immunity and the cancer-immune set point. *Nature*. 2017;541:321–330. https://doi.org/10.1038/nature21349
12. Galon J, Bruni D. Approaches to treat immune hot, altered and cold tumours with combination immunotherapies. *Nat Rev Drug Discov*. 2019;18:197–218. https://doi.org/10.1038/s41573-018-0007-y
13. Perrone AM, Di Marcoberardino B, Rossi M, et al. Laparoscopic versus laparotomic approach to endometrial cancer. *Eur J Gynaecol Oncol*. 2012;33:376–381. PMID: 23091894.
14. Cho KR, Cooper K, Croce S, et al. International Society of Gynecological Pathologists (ISGyP) endometrial cancer project: guidelines from the special techniques and ancillary studies group. *Int J Gynecol Pathol*. 2019;38(Suppl 1):S114–S122. https://doi.org/10.1097/PGP.0000000000000496
15. WHO Classification of Tumours. *Female Genital Tumours*. 5th ed. Vol 4. IARC; 2020.
16. Soslow RA, Tornos C, Park KJ, et al. Endometrial carcinoma diagnosis: use of FIGO grading and genomic subcategories in clinical practice: recommendations of the International Society of Gynecological Pathologists. *Int J Gynecol Pathol*. 2019;38(Suppl 1):S64–S74. https://doi.org/10.1097/PGP.0000000000000518
17. Creasman W. Revised FIGO staging for carcinoma of the endometrium. *Int J Gynaecol Obstet*. 2009;105:109. https://doi.org/10.1016/j.ijgo.2009.02.010
18. Bosse T, Peters EE, Creutzberg CL, et al. Substantial lymph-vascular space invasion (LVSI) is a significant risk factor for recurrence in endometrial cancer—a pooled analysis of PORTEC 1 and 2 trials. *Eur J Cancer*. 2015;51:1742–1750. https://doi.org/10.1016/j.ejca.2015.05.015
19. Fujimoto T, Nanjyo H, Fukuda J, et al. Endometrioid uterine cancer: histopathological risk factors of local and distant recurrence. *Gynecol Oncol*. 2009;112:342–347. https://doi.org/10.1016/j.ygyno.2008.10.019
20. Murray SK, Young RH, Scully RE. Unusual epithelial and stromal changes in myoinvasive endometrioid adenocarcinoma: a study of their frequency, associated diagnostic problems, and prognostic significance. *Int J Gynecol Pathol*. 2003;22:324–333. https://doi.org/10.1097/01.pgp.0000092161.33490.a9
21. Euscher E, Fox P, Bassett R, et al. The pattern of myometrial invasion as a predictor of lymph node metastasis or extrauterine disease in low-grade endometrial carcinoma. *Am J Surg Pathol*. 2013;37:1728–1736. https://doi.org/10.1097/PAS.0b013e318299f2ab
22. Kobel M, Ronnett BM, Singh N, Soslow RA, Gilks CB, McCluggage WG. Interpretation of P53 immunohistochemistry in endometrial carcinomas: toward increased reproducibility. *Int J Gynecol Pathol*. 2019;38(Suppl 1):S123–S131. https://doi.org/10.1097/PGP.0000000000000488
23. Singh N, Piskorz AM, Bosse T, et al. p53 immunohistochemistry is an accurate surrogate for TP53 mutational analysis in endometrial carcinoma biopsies. *J Pathol*. 2020;250:336–345. https://doi.org/10.1002/path.5375
24. McConechy MK, Talhouk A, Li-Chang HH, et al. Detection of DNA mismatch repair (MMR) deficiencies by immunohistochemistry can effectively diagnose the microsatellite instability (MSI) phenotype in endometrial carcinomas. *Gynecol Oncol*. 2015;137:306–310. https://doi.org/10.1016/j.ygyno.2015.01.541
25. Stelloo E, Jansen AML, Osse EM, et al. Practical guidance for mismatch repair-deficiency testing in endometrial cancer. *Ann Oncol*. 2017;28:96–102. https://doi.org/10.1093/annonc/mdw542
26. Ceccarelli C, De Leo A, Chieco P, et al. A simple immunohistochemical bioprofile incorporating Bcl2 curbs those cases of invasive breast carcinoma for which an Oncotype Dx characterization is needed. *PLoS One*. 2019;14, e0217937. https://doi.org/10.1371/journal.pone.0217937
27. de Biase D, Acquaviva G, Visani M, et al. Molecular diagnostic of solid tumor using a next generation sequencing custom-designed multi-gene panel. *Diagnostics (Basel)*. 2020;10:250. https://doi.org/10.3390/diagnostics10040250
28. De Leo A, Ravegnini G, Musiani F, et al. Relevance of ARID1A mutations in endometrial carcinomas. *Diagnostics (Basel)*. 2022;12:590. https://doi.org/10.3390/diagnostics12030592
29. Integrative Genomics Viewer 2.12.2 (IGV) tool. Available online http://software.broadinstitute.org/software/igv/. accessed on 15th April 2024
30. The Varsome tool. https://varsome.com/. accessed on 15th April 2024.
31. Kopanos C, Tsiolkas V, Kouris A, et al. VarSome: the human genomic variant search engine. *Bioinformatics*. 2019;35:1978–1980. https://doi.org/10.1093/bioinformatics/bty897
32. Leon-Castillo A, Britton H, McConechy MK, et al. Interpretation of somatic POLE mutations in endometrial carcinoma. *J Pathol*. 2020;250:323–335. https://doi.org/10.1002/path.5372
33. Huvila J, Thompson EF, Vanden Broek J, et al. Subclonal p53 immunostaining in the diagnosis of endometrial carcinoma molecular subtype. *Histopathology*. 2023;83:880–890. https://doi.org/10.1111/his.15029
34. Gehan EA. A generalized Wilcoxon test for comparing arbitrarily singly-censored samples. *Biometrika*. 1965;52:203–223. https://doi.org/10.2307/2333825
35. Breslow N. A generalized Kruskal–Wallis test for comparing K samples subject to unequal patterns of censorship. *Biometrika*. 1970;57:579–594. https://doi.org/10.2307/2334776
36. Graf E, Schmoor C, Sauerbrei W, Schumacher M. Assessment and comparison of prognostic classification schemes for survival data. *Stat Med*. 1999;18:2529–2545. https://doi.org/10.1002/(sici)1097-0258(19990915/30)18:17/18<2529::aid-sim274>3.0.co;2-5
37. Grambsch PM, Therneau TM. Proportional hazards tests and diagnostics based on weighted residuals. *Biometrika*. 1994;81:515–526. https://doi.org/10.2307/2337123
38. Benjamini Y, Yekutieli D. The control of the false discovery rate in multiple testing under dependency. *Ann Stat*. 2001;29:1165–1188. https://doi.org/10.1214/aos/1013699998
39. Gonzalez H, Hagerling C, Werb Z. Roles of the immune system in cancer: from tumor initiation to metastatic progression. *Genes Dev*. 2018;32:1267–1284. https://doi.org/10.1101/gad.314617.118
40. Hiam-Galvez KJ, Allen BM, Spitzer MH. Systemic immunity in cancer. *Nat Rev Cancer*. 2021;21:345–359. https://doi.org/10.1038/s41568-021-00347-z
41. Hegde PS, Chen DS. Top 10 challenges in cancer immunotherapy. *Immunity*. 2020;52:17–35. https://doi.org/10.1016/j.immuni.2019.12.011
42. Joyce JA, Fearon DT. T cell exclusion, immune privilege, and the tumor microenvironment. *Science*. 2015;348:74–80. https://doi.org/10.1126/science.aaa6204
43. Tiwari A, Oravecz T, Dillon LA, et al. Towards a consensus definition of immune exclusion in cancer. *Front Immunol*. 2023;14, 1084887. https://doi.org/10.3389/fimmu.2023.1084887
44. Stewart CJ, Little L. Immunophenotypic features of MELF pattern invasion in endometrial adenocarcinoma: evidence for epithelial–mesenchymal transition. *Histopathology*. 2009;55:91–101. https://doi.org/10.1111/j.1365-2559.2009.03327.x
45. Kondratiev S, Sabo E, Yakirevich E, Lavie O, Resnick MB. Intratumoral CD8+ T lymphocytes as a prognostic factor of survival in endometrial carcinoma. *Clin Cancer Res*. 2004;10:4450–4456. https://doi.org/10.1158/1078-0432.CCR-0732-3
46. de Jong RA, Leffers N, Boezen HM, et al. Presence of tumor-infiltrating lymphocytes is an independent prognostic factor in type I and II endometrial cancer. *Gynecol Oncol*. 2009;114:105–110. https://doi.org/10.1016/j.ygyno.2009.03.022
47. Talhouk A, Derocher H, Schmidt P, et al. Molecular subtype not immune response drives outcomes in endometrial carcinoma. *Clin Cancer Res*. 2019;25:2537–2548. https://doi.org/10.1158/1078-0432.CCR-18-3241
48. Horeweg N, de Bruyn M, Nout RA, et al. Prognostic integrated image-based immune and molecular profiling in early-stage endometrial cancer. *Cancer Immunol Res*. 2020;8:1508–1519. https://doi.org/10.1158/2326-6066.CIR-20-0149
49. Lopez-Janeiro A, Villalba-Esparza M, Brizzi ME, et al. The association between the tumor immune microenvironments and clinical outcome in low-grade, early-stage endometrial cancer patients. *J Pathol*. 2022;258:426–436. https://doi.org/10.1002/path.6012
50. Wang XQ, Danenberg E, Huang CS, et al. Spatial predictors of immunotherapy response in triple-negative breast cancer. *Nature*. 2023;621:868–876. https://doi.org/10.1038/s41586-023-06498-3
51. Backman M, Strell C, Lindberg A, et al. Spatial immunophenotyping of the tumour microenvironment in non-small cell lung cancer. *Eur J Cancer*. 2023;185:40–52. https://doi.org/10.1016/j.ejca.2023.02.012
52. Shen J, Choi YL, Lee T, et al. Inflamed immune phenotype predicts favorable clinical outcomes of immune checkpoint inhibitor therapy across multiple cancer types. *J Immunother Cancer*. 2024;12:1–13. https://doi.org/10.1136/jitc-2023-008339
53. Rodriguez JA. HLA-mediated tumor escape mechanisms that may impair immunotherapy clinical outcomes via T-cell activation. *Oncol Lett*. 2017;14:4415–4427. https://doi.org/10.3892/ol.2017.6784